Laboratory investigation of non-steady penetrative convection

By J. W. DEARDORFF, G. E. WILLIS AND
D. K. LILLY

National Center for Atmospheric Research, Boulder, Colorado

Laboratory experiments of non-steady penetrative convection in water are performed that closely simulate the lifting of an atmospheric inversion above heated ground. Vertical profiles of horizontally averaged temperature and heat flux are measured and interpreted. The rate at which kinetic energy is destroyed by the downward heat flux in the vicinity of the inversion base is found to be a very small fraction of the rate at which it is generated in the lower convective region. The interface separating the convective region from the stable region is examined and its rate of rise explained.

1. Introduction

Penetrative convection concerns the advance of a turbulent fluid into a fluid layer of stable stratification. Its study is of importance in several areas of geophysical fluid dynamics, with perhaps the most emphasis occurring for cases of the upper ocean and the lower atmosphere. The upper ocean case is discussed in some detail by Phillips (1966).

The phenomenon occurs in the atmosphere chiefly in two forms. In one, a relatively isolated buoyant element (either bubble or plume) may penetrate upwards into a surrounding stable atmosphere. In this case, the surrounding atmosphere may be considered to be scarcely affected by the growing element, with no immediate interaction except for modification of the air entrained through the boundaries of the element. Then one may examine the effect of a given environment upon the element's growth and history. This subject has been treated in both theoretical and laboratory or atmospheric studies. A large number of references to such investigations may be found in Priestley (1959, chapter 6), with some more recent references in Telford (1967).

In the other form, a turbulent convective fluid covers a large horizontal area, and may gradually deepen and incorporate a stable fluid layer above it. This phenomenon is commonly observed when, owing to surface heating, a nocturnal inversion is replaced from below by a growing unstable layer adjacent to the ground. In this case, the initially stable environment near the ground is obviously affected by the convection, and full interaction between the two regions occurs. The convection may still be termed penetrative because the front of the advancing unstable layer is known to have domes which penetrate small distances into the stable layer. This form of convection, to be investigated here, has been

the subject of some observational study (Lettau & Davidson 1957; Izumi 1964; Deardorff 1967; Lenschow & Johnson 1968), and of some theoretical modelling (Ball 1960; Veronis 1963; Kraus & Turner 1967; Lilly 1968). However, the phenomenon has not received much detailed laboratory study.

The laboratory study of Rouse & Dodu (1955) showed that a density discontinuity between two adjacent fluid layers will locally remain a sharply defined interface, even after one of the layers is stirred mechanically. The incorporation of the non-turbulent lower fluid into the turbulent upper fluid took place at the region of the interface with the 'lower layer remaining otherwise undisturbed'. This entrainment was observed to occur in streamers emanating from cusps at the interface. The rate of entrainment was related to the density difference and stirring rate. It is difficult, however, to apply this result to a more natural system, in which the energy input is by means of a shear stress or heat flux existing throughout a layer of appreciable depth.

A similar experiment was performed by Cromwell (1960), except that the stable stratification was associated with a density decreasing continuously with height over a 15 cm height. As the mixing proceeded, a continuously sharpening interface did develop, and the entrainment mechanism appears to have been the same as that described by Rouse & Dodu. The density difference across the interface increased with time, and was roughly equal to one-half the product of the initial density gradient and interface depth.

A refinement of Cromwell's experiment was recently performed by Kato (1967). Mechanical stirring was replaced by application of a constant and known stress at one boundary. The interface depth was found to be proportional to $u_* \tau_B^{\frac{1}{2}} t^{\frac{1}{2}}$, where u_* is the friction velocity, τ_B the initial Brunt–Väisälä period, and t is time.

In an experiment by Townsend (1964), a tank of water, initially isothermal, was cooled from below and heated gently from above. The lower boundary became cooler than the temperature of maximum density, 4 °C, so that an unstable layer developed adjacent to the bottom. As it thickened, a stable layer developed above it; and, at the end of the experiment, an equilibrium was approached in which the laminar heat flux directed downward through the stable layer nearly equalled the value of the downward turbulent flux below. The experiment disclosed several interesting facts. Except in the lowest few centimetres, the temperature fluctuations were of maximum amplitude at the level of the mean interface, or slightly above it. In the upper stable region these fluctuations appeared to be associated with internal waves excited by the impacts from below of penetrating and subsequently subsiding columns. Their amplitude decreased rapidly with further increase of height. The boundary heat flux was related through a universal constant to the mean temperature difference between the lower boundary and the mixed region. However, this flux, as measured, say, by a characteristic Nusselt number of the mixed region, was relatively small. Additional measurements of the constant for more intense penetrative convection, and for a less variable coefficient of thermal expansion, are desirable. It should also be noted that this experiment was basically different from the atmospheric case in that the heat flux was nearly constant with height.

The density structure of the upper ocean was simulated by Turner & Kraus (1967) in an experiment in which continuous mechanical stirring and occasional additions of lighter or denser fluids were applied to the upper boundary of a tank of salt water. The rates at which the density interfaces descended, which equalled the entrainment rates, were observed and hypothesized to be a function of the surface stress or stirring rate, density difference, and depth to the interface. Several seasonal changes of the oceanic thermocline were successfully modelled. The theory used to explain these changes assumed negligible dissipation of kinetic energy by viscosity, an assumption which we believe is questionable.

In the present experiments, the stratification of the stable layer is distributed continuously and nearly uniformly throughout the layer, as in Townsend's and Cromwell's experiments. But unlike Cromwell's experiment the energy input is by heat flux at one boundary, rather than by arbitrary stirring. In contrast to Townsend's experiment, the boundary heat flux is directed into the convective layer and decreases towards the stable interface. The mean thermal structure is consequently non-steady and the convective layer continually deepens. Also, in contrast to Townsend's experiment, the stratification within the stable layer remains essentially constant while the interface rises.

2. Equipment and experimental procedure

The fluid used was distilled water, rather than air, in order to allow both a rather large heating rate and sufficient time to take measurements of the changing thermal structure. The container, as shown in figure 1, was a cylindrical tank with an inside diameter of 54·8 cm and a height of 35·5 cm. Its side walls were insulated by 1·3 cm of sponge rubber on the inside and by 1·3 cm of sponge rubber plus 3·8 cm of fibreglass insulation on the outside. A metal tray containing a circulating water bath at constant temperature was in contact with the upper surface of the distilled water to provide a nearly constant upper boundary temperature. The lower boundary of the container was an aluminium disk of thickness 0·63 cm in thermal contact with copper coils underneath. The coils contained circulating water from another constant-temperature bath. The lower side of the coils was insulated by 1·3 cm of sponge rubber plus 2·5 cm of styrofoam.

For measuring mean temperature at various heights, a long resistance wire of length 510 cm was strung back and forth across a horizontal brass ring support of inner diameter 52 cm and thickness 0·24 cm, as shown in figure 2. The wire was located on the ring in such a manner that the ratio of wire length in a given annulus to the area of that annulus was nearly constant. The wire served as one arm of a d.c. bridge-circuit so that changes in the off-balance voltage were proportional to the variations of horizontally averaged temperature. The platinum-alloy resistance wire had a diameter of 0·005 cm, with its time constant, based on a relative water velocity of 1·0 cm sec^{-1}, estimated to be 4 msec. Located in the same plane as the resistance wire were two thermocouples (denoted in figure 2 by circled ×), one in the centre of the container and the other at a radius of 19·3 cm. Their time constant was estimated to be 40 msec. The ring support could be moved vertically at a nearly constant rate of 1·0 cm sec^{-1}
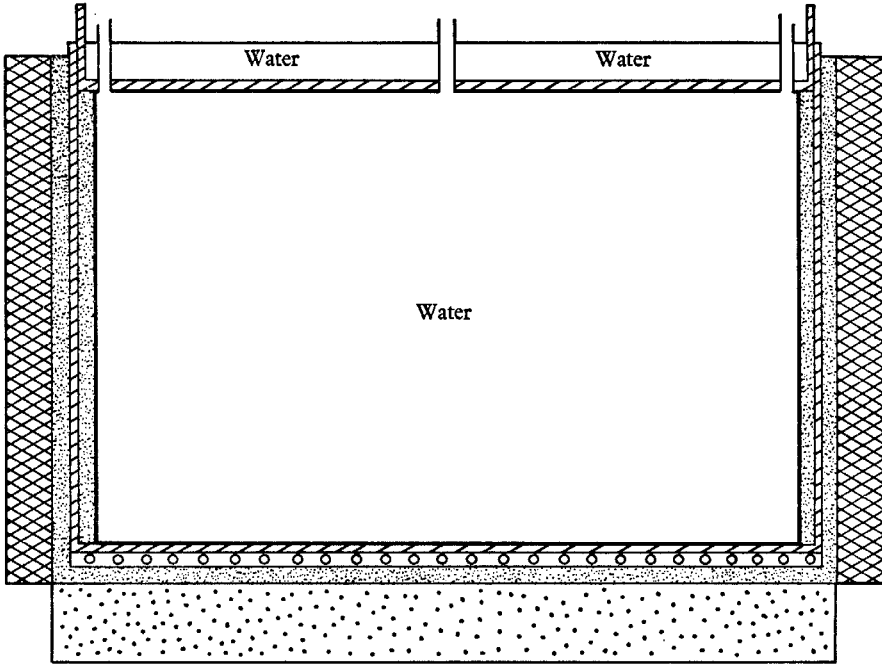
FIGURE 1. The penetrative-convection container with circulating warm water in a metal tray on top, and circulating cool or warm water in coils underneath.
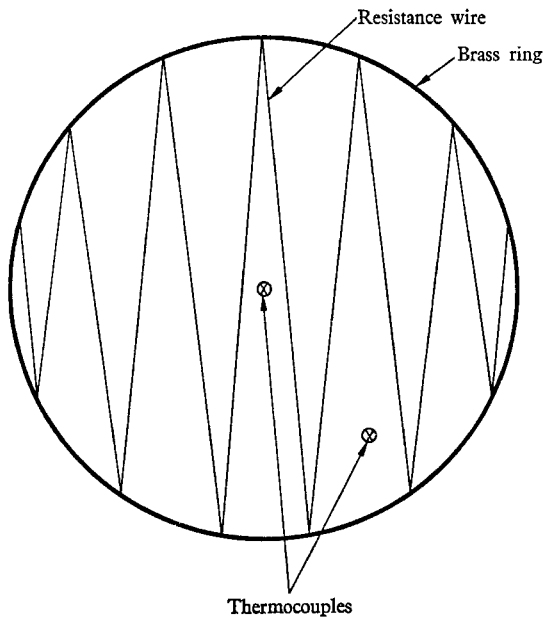

FIGURE 2. The vertically moving probe, with resistance wire and two thermocouples.

upwards and 1·1 cm sec⁻¹ downwards by a motor with its gear drive located directly above the upper tray of water. Several short vertical tubes of small diameter within the upper bath allowed three support tubes of diameter 0·32 cm to connect the resistance-wire supporting ring to the motor drive. They also provided access for electrical connexions.

By means of two microswitches mounted near the motor drive, the motor could be operated continuously and reversed periodically to recycle the resistance wire from a level 0·8 ± 0·1 cm above the bottom to within 3·1 ± 0·1 cm of the upper boundary and back again. The time of each actuation of a microswitch (and hence the level of the resistance wire at this time) was monitored by an event marker on the same strip-chart trace used for the mean temperature. A

Designation of experiment	T_{b0} (°C)	T_{bm} (°C)	$(\partial \bar{T}/\partial z)_0$ (°C cm⁻¹)	Time required for $h_t = 27 \cdot 5$ cm (min)	τ_B (sec)
A	21·5	43·4	0·45	6·8	17·4
B	29·6	40·7	0·21	7·3	23·7
C	21·3	39·2	0·47	15·2	16·8

TABLE 1

two-channel Offner Dynagraph was used as the amplifier-recorder. The second channel of this recorder monitored the temperature of the lower boundary as sensed by a copper–constantan thermocouple in contact with the bottom aluminium disk. Another dual-channel recorder monitored the signals of the thermocouples, which moved along with the resistance wire.

The fluid initial conditions were zero velocity and a continuous, approximately linear, temperature increase with height. At the upper boundary, $z = h$, the temperature was maintained at about 39 °C. At the lower boundary, three initial temperatures, T_{b0}, were used as indicated in table 1. The continuous initial-temperature condition was attained by filling the tank slowly at the level of a floating plywood disk with successive increments of warmer water, and allowing the resulting steps to smooth out over a period of about 6 h. This length of time was sufficient to eliminate most of the curvature in the temperature profile except near the upper boundary, where some increased stirring occurred as the plywood disk was removed. The experiments to be presented were terminated before the warming reached this level.

The thermal convection was initiated at time $t = 0$ upon replacing the cool water circulating under the lower boundary with warm water of temperature greater than the upper boundary temperature. Within 2 min the bottom temperature, T_b, increased rapidly to at least 82 % of its final value and thereafter gradually approached the final value. An average bottom temperature, T_{bm}, listed in table 1, was taken as the mean over the time interval of heat-flux pro-files to be presented. The temperature T_b at any time was not quite uniform horizontally, but generally increased about 0·3 °C from the centre of the disk to near the outer edge.

During an experiment the resistance wire was cycled repeatedly to obtain successive mean temperature profiles. A test was performed to determine the effect, if any, which movement of the resistance wire and its supporting ring would have upon the mean temperature structure. Since any effect would be most serious in the absence of natural motions, the test was performed while the water was still entirely stratified, with $T_b = T_{b0}$. The resistance wire was cycled 30 times at the same rate as during an experiment, and the consecutive mean profiles obtained differed imperceptibly in shape, although a slow apparent drift in
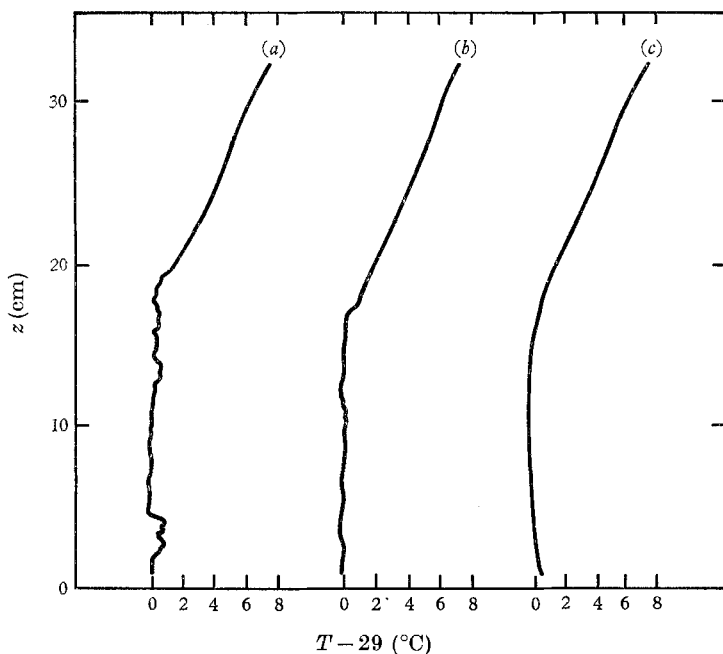

FIGURE 3. Typical vertical profiles of temperature from two thermocouples, (a) and (b), and from the resistance wire, (c), during an upward traverse of experiment A.

mean temperature occurred. Any stirring by the sensor and support should have tended to decrease the temperature gradient in the region of sensor movement, and increase gradients near the boundaries. Since this effect was absent, it was concluded that the sensor and probe movement did not cause any significant mixing of the water. This result is not unexpected since the average Reynolds number of the moving resistance wire is about 1 and that of the support ring about 35. However, a significant drift did exist in either the recorder zero-position or the resistance wire bridge-balance, or both. Hence, in analysing the experimental observations, corrections were applied to the data to eliminate any long-term drift by assuming that the mean temperature near the top at $z = 32.4$ cm was constant with time. The average temperature correction between successive profiles was $0.007\ °C$.

The results of a single upward traverse of the probe with the interface at a height of about 19 cm are shown in figure 3. Curve (a) is the trace from the thermocouple located along the vertical axis of the container; curve (b) is from

the thermocouple located at a radius of 19·3 cm; and curve (c) is that of the resistance wire. Temperature fluctuations of magnitude 0·5 °C are present in the thermocouple traces, while fluctuations of this nature are virtually absent from the resistance wire output owing to the temperature being averaged over the entire length of the resistance wire. It is evident that mean-value calculations performed from the resistance wire data are subject to considerably less sampling error than those from thermocouple data, while the latter more effectively bring out details of the sharp turbulent interface.

In one series of experiments the resistance wire and several thermocouples were maintained at fixed heights throughout the experiment in order to estimate the temperature variance at these heights. These experiments were similar to either *A* or *C* except that boundary heat fluxes were slightly smaller.

Some preliminary visual experiments with dyes were performed (in a rectangular, plexiglass tank with horizontal dimensions 50 × 50 cm and height 35 cm); and qualitative observations from these experiments will be introduced in this paper. Essentially, two kinds of dye experiments were performed, one to view the movement and shape of the interface, the second to observe the water entraining into the convective layer.

3. Methods of data analysis

Each mean-temperature profile to be presented was first obtained as an average of four consecutive traverses of the resistance wire: upwards, downwards, upwards and downwards, in that order. Hence each profile is centred at the same time at each level, but is an average over about 2 min near the bottom and 1 min near the top. Each profile is, furthermore, an average over three experiments, each with nearly the same initial conditions. Corrections were applied to the original temperatures for instrumental zero-drifts as previously described.

The heights to which the mean temperatures $\overline{T}$ apply were obtained from knowledge of the average resistance-wire height when the event-marker microswitches near the terminals of a traverse were tripped, and by assuming a linear travel speed and recorder chart speed between these points. There was no indication that these assumptions were in significant error, as the motor acceleration for each traverse occurred almost entirely before the initial event-marker microswitch was triggered, and the subsequent deceleration occurred entirely after the final event-marker microswitch was triggered. Data gathered when the probe speed was not uniform were not used in the analysis. The height limits used (as measured from the lower boundary) were 1·3 cm and 32·4 cm.

Mean temperatures were digitized at height intervals of 0·305 cm, with subsequent vertical averaging giving a height interval of 0·61 cm between data points of profiles to be presented. Subsequent calculations were performed by digital computer.

The heat flux H at level z was obtained by numerical integration of the thermal diffusion equation

$$\left(\frac{H}{\rho c}\right)_z = \left(\frac{H}{\rho c}\right)_h + \int_z^h \frac{\partial \overline{T}}{\partial t}\, dz, \tag{1}$$

where ρ is the water density and c its specific heat. In actual practice, level h in (1) was not the upper boundary height, but was the upper limit of each traverse, 32·4 cm. At this latter level, H was assumed to be due to molecular transfer. This assumption is not believed to have led to serious error except after the interface had approached within about 5 cm of this level. The time derivative in (1) was taken over an interval of 1 min.

Except in the experiments using dye, the interface itself was not directly observed. Its mean height had to be inferred from either the mean temperature profile or from the heat flux profile. From measurements to be presented, we found that some cooling occurs at a given point before the local interface reaches that point, with maximum cooling coinciding with the presence of the local interface. Hence a good definition of the mean interface height is the level of maximum mean cooling. It is easily shown that this level coincides with the level of maximum downward heat transport. Since this latter level is quite well defined (see figures 7–9), it will be used here as the definition of the mean interface height.

The data of the experiment with stationary sensors were digitized at 1 sec intervals. After removal of any long-term trend, each computed value of the temperature variance was taken as the average of T'^2 over a period of 40 sec, where T' is the fluctuation of T from a mean over this interval. In addition, each value of variance was an average from two thermocouples, one located on the centre line of the container and the other at a radius of 21·2 cm.

4. Results and discussion

Three different sets of initial conditions were investigated, as listed in table 1. The mean initial temperature gradient, $(\partial \bar{T}/\partial z)_0$, was determined by taking the best-fitting straight line from the initial mean profiles over the height of probe travel. The subscript i is taken to mean the interface. The Brunt–Väisälä period, τ_B, also listed was computed from

$$\tau_B = 2\pi \left[g\alpha \left(\frac{\partial \bar{T}}{\partial z} \right)_0 \right]^{-\frac{1}{2}},$$

where α is the volume coefficient of thermal expansion evaluated at the initial mean temperature at a height of 20 cm, and g is the gravitational acceleration.

4.1. *Mean temperature profiles*

Mean profiles of T for cases A, B and C are shown in figures 4, 5 and 6, respectively. For clarity, only every other profile is shown in the slower experiment, C. The labels on profiles represent minutes from the beginning of each experiment. A dimensionless temperature T^* has been used for the lower abscissa scale.† It is defined by
$$T^* = (\bar{T} - T_{b0})/(T_{bm} - T_{b0}), \tag{2}$$

where $\bar{T}$ is the mean temperature (horizontally averaged), T_{b0} the initial value of T_b, and T_{bm} the mean of T_b already defined.

The height scale on the left-hand ordinate is also dimensionless, and is defined by
$$z^* = (T_{bm} - T_{b0})^{-1} (\partial \bar{T}/\partial z)_0 z. \tag{3}$$

† The superscripted asterisk will denote quantities which have been made dimensionless.

An intense lapse rate (not measured) exists below the lowest level of measurement, with $T^* = 1$ at $z^* = 0$. The well-mixed, nearly isothermal region commences above this level, and increases in depth as the experiment progresses. The lapse rate becomes slightly stable well before the inversion base is reached. The pronounced counter-gradient slopes of the first two profiles after the initial one
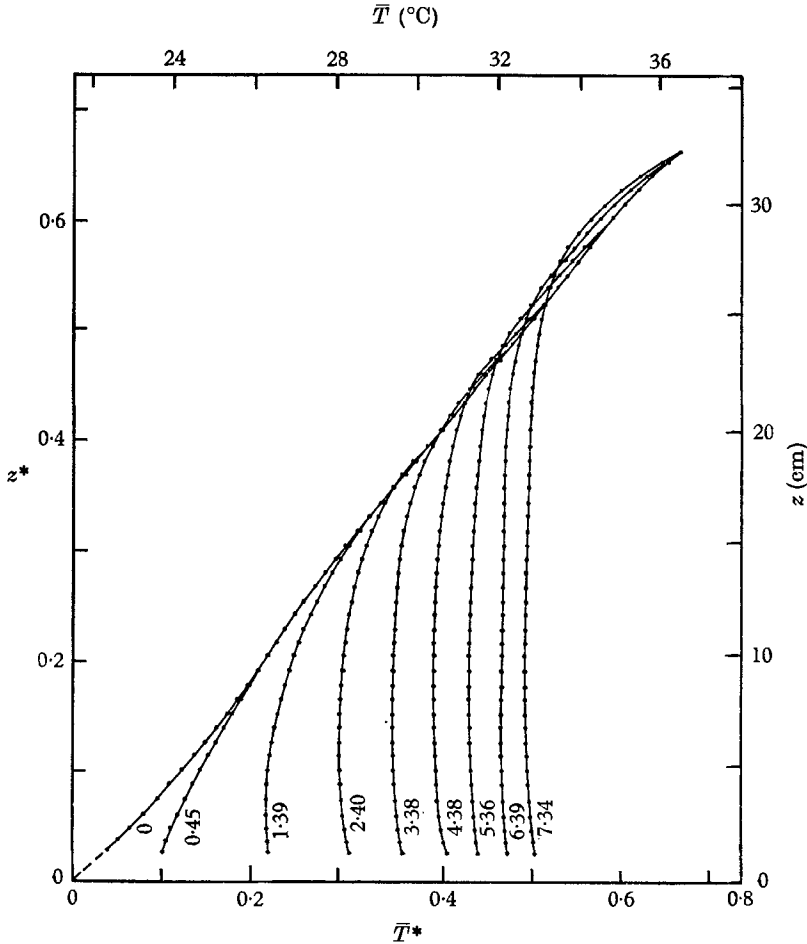

FIGURE 4. Vertical profiles of horizontally averaged temperature for experiment A. Profile labels give time in minutes. Dimensionless scales are on bottom and left, dimensional scales on top and right.

in each experiment are mostly fictitious and arise from the use of time averages when the interface was rising rapidly. However, the counter-gradient slopes of subsequent profiles are definitely real and extend from a level somewhat below the interface down to $z^* \simeq 0.3$. There is no peaked layer of minimum temperature just below the inversion, as was found by Townsend (1964) when measuring temperatures along a single column in the centre of his convection tank. However, a slight cooling occurs at a given level just before the interface reaches that level,

especially after the experiment has proceeded several minutes. This cooling causes the base of the stable layer to be slightly more stable than initially.

An important difference can now be seen to exist between our experiment and one with mechanical stirring but no heat or mass input. For example, in Cromwell's (1960) experiment, a large density decrease necessarily occurred near the
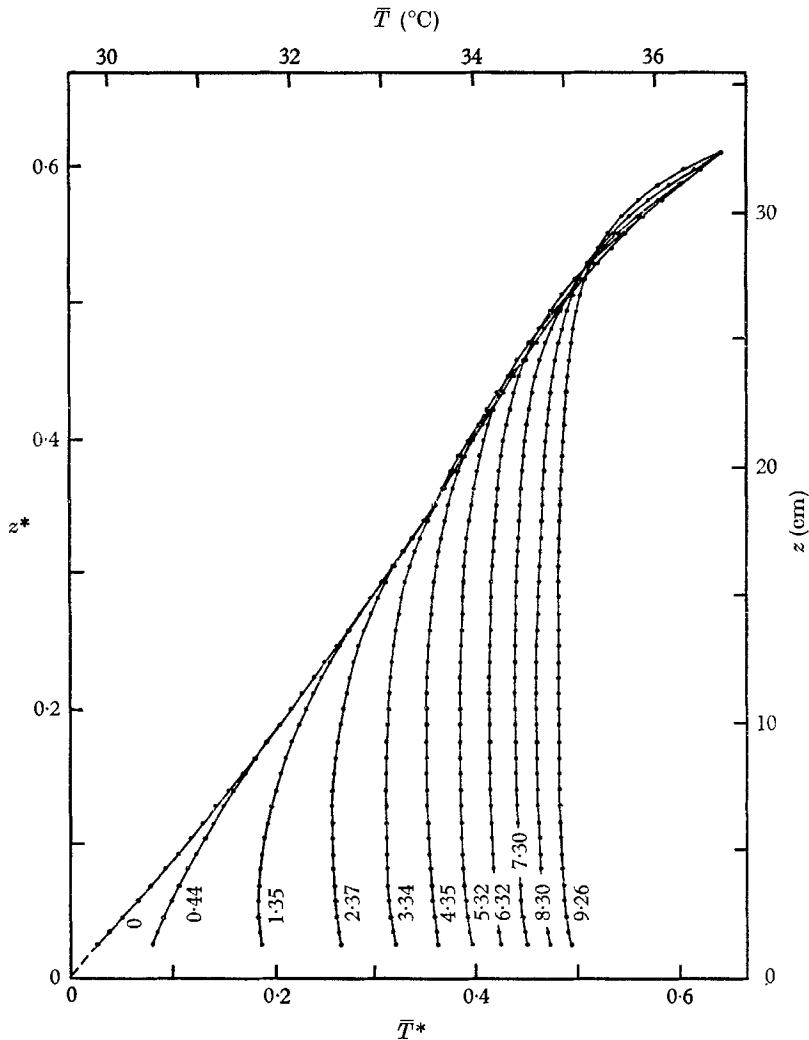

FIGURE 5. Same as figure 4, but for experiment *B*.

interface level to compensate the equally large increase near the surface as the mechanical stirring at the top produced a thickening constant-density layer. The compensation resulted from the absence of any density sources or sinks. In our experiment, the heat input at the lower boundary allows the temperature of the well-mixed layer to increase with very little compensating cooling at the interface level.

4.2. *Heat flux profiles*

Corresponding profiles of dimensionless heat flux are presented in figures 7, 8 and 9, where successive profiles are drawn with solid, dashed and dotted lines. The elapsed time for each profile is given in table 2. The dimensionless fluxes are defined by

$$(H/\rho c)^* = (g\alpha\kappa^2/\nu)^{-\frac{1}{3}}(T_{bm}-T_{b0})^{-\frac{4}{3}}(H/\rho c), \tag{4}$$
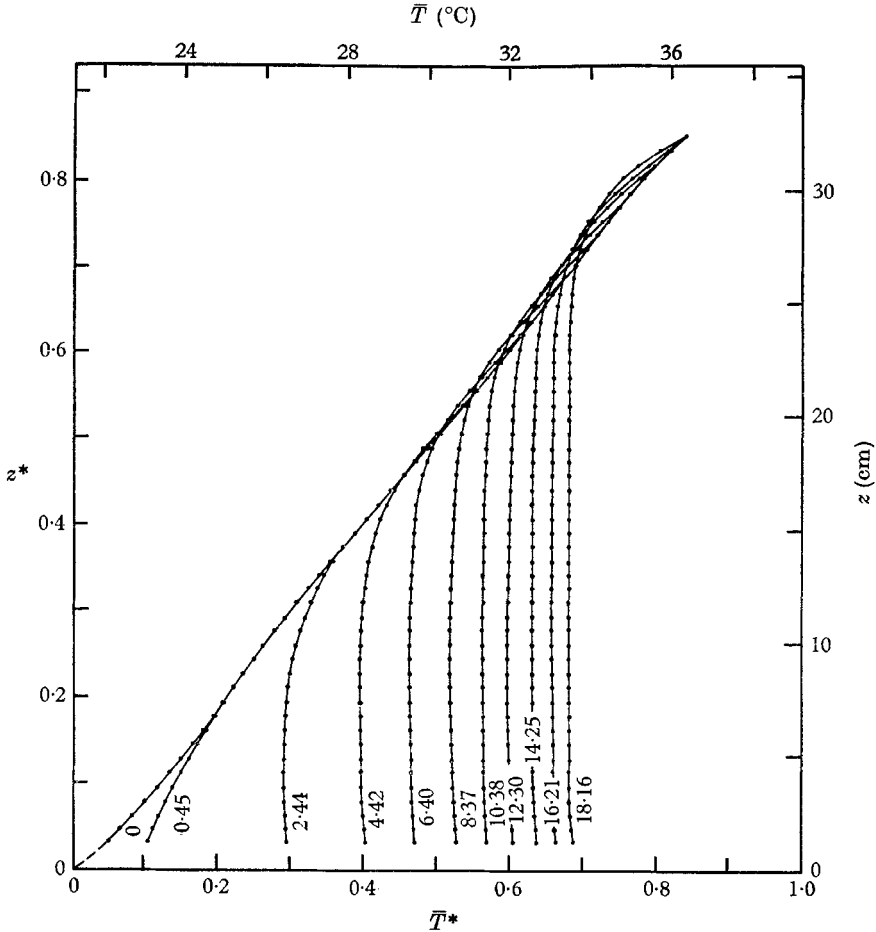

FIGURE 6. Same as figure 4, but for experiment *C*.

where κ and ν are the thermal diffusivity and kinematic viscosity, respectively, evaluated at the temperature existing at mid-level during initial conditions.

The reason for making quantities dimensionless in this manner will be made apparent in §4.3, although whenever feasible the dimensional scales are also given on the figures. It may be noticed that (2), (3) and (4) together indicate that a dimensionless time is correspondingly defined by

$$t^* = \left(g\alpha\frac{\kappa^2}{\nu}\right)^{\frac{1}{3}}\left(\frac{\partial\overline{T}}{\partial z}\right)_0(T_{bm}-T_{b0})^{-\frac{2}{3}}t. \tag{5}$$

The heat flux is seen to decrease linearly with height in the lowest levels, reflecting the fact that the mean temperature profile within the mixed region retains an almost isothermal shape as warming proceeds. Generally, the heat flux re-
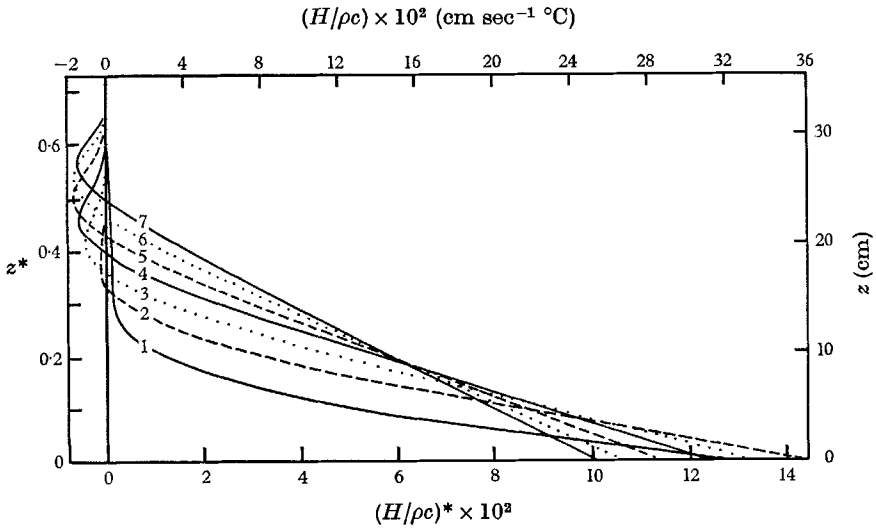
$$(H/\rho c) \times 10^2 \ (\text{cm sec}^{-1} \ {}^\circ\text{C})$$

FIGURE 7. Vertical profiles of heat flux for experiment A, with labels giving time in minutes. Dimensionless scales are on bottom and left, dimensional scales on top and right.

$$(H/\rho c) \times 10^2 \ (\text{cm sec}^{-1} \ {}^\circ\text{C})$$
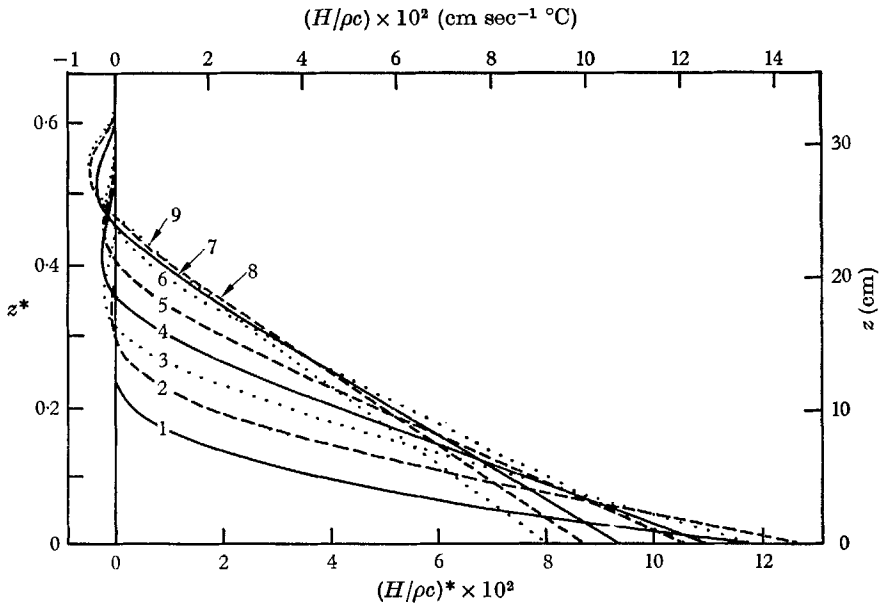
FIGURE 8. Same as figure 7, but for experiment B.

verses sign from plus to minus a small distance, ($\Delta z^* \simeq 0{\cdot}1$), below the mean interface. The negative heat-flux area is nearly non-existent early in each experiment, but becomes more pronounced as the interface rises. (The tiny positive heat flux extending to large heights for curve 1 in figure 7 is probably an error
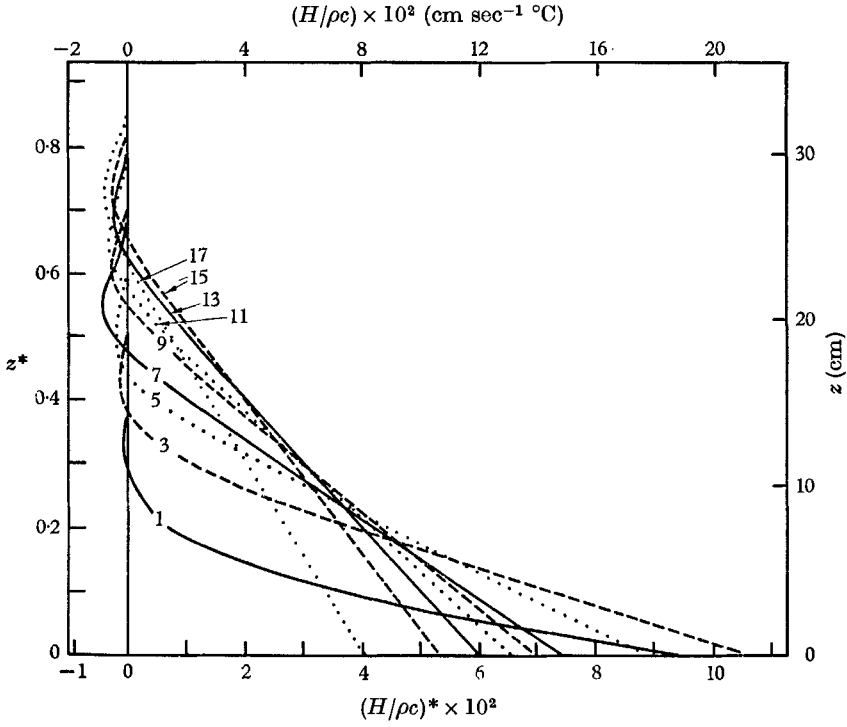
FIGURE 9. Same as figure 7, but for experiment *C*.

Profile	Experiment *A*			Experiment *B*			Experiment *C*		
	Time (min)	*R*	*C*	Time (min)	*R*	*C*	Time (min)	*R*	*C*
1	0·92	—	0·250	0·89	0·002	0·219	0·96	0·003	0·250
2	1·89	0·005	0·265	1·86	0·003	0·238	1·94	0·002	0·257
3	2·89	0·020	0·238	2·86	0·010	0·208	2·94	0·006	0·242
4	3·88	0·027	0·226	3·85	0·015	0·205	3·93	0·010	0·227
5	4·85	0·032	0·221	4·84	0·009	0·203	4·94	0·010	0·216
6	5·85	0·023	0·214	5·82	0·005	0·209	5·92	0·011	0·216
7	6·81	0·026	0·212	6·80	0·013	0·195	6·90	0·026	0·199
8	—	—	—	7·80	0·020	0·185	7·87	0·017	0·207
9	—	—	—	8·79	0·018	0·178	8·86	0·011	0·203
10	—	—	—	—	—	—	9·85	0·017	0·207
11	—	—	—	—	—	—	10·81	0·019	0·213
12	—	—	—	—	—	—	11·80	0·017	0·201
13	—	—	—	—	—	—	12·80	0·012	0·213
14	—	—	—	—	—	—	13·78	0·026	0·194
15	—	—	—	—	—	—	14·73	0·013	0·200
16	—	—	—	—	—	—	15·71	0·016	0·186
17	—	—	—	—	—	—	16·67	0·038	0·160
18	—	—	—	—	—	—	17·61	0·024	0·180

TABLE 2

caused by a changing instrumental drift rate early in that experiment.) The ratio of the area enclosed by negative heat flux to that of positive flux, R, is tabulated in table 2. This ratio signifies what fraction of kinetic energy generated by buoyancy in the unstable region is being used to increase the potential energy associated with downward entrainment of the upper warm water, with consequent lifting of the interface.

It was assumed by Ball (1960) that $R \simeq 1$, which requires for the atmosphere that the rate of viscous dissipation of kinetic energy, ϵ, be either negligible or at most balanced by its rate of production by wind shear. In our experiment, this assumption would require that ϵ at most equal the net rate of increase of kinetic energy, which was not measured. The very small values of R in table 2, with an average magnitude of about 0·015, indicate only that the net production rate of energy by the heat flux was almost balanced by the combination of viscous dissipation and kinetic energy increase. However, the similarity of this type of convection to parallel-plate convection, in which ϵ generally balances the production by buoyancy, and our order-of-magnitude estimates of kinetic energy increase both indicate that viscous dissipation was the more important factor here, which counterbalanced the energy production by buoyancy. The assumption by Turner & Kraus (1967) that ϵ was a negligible item in the energy budget of their experiment thus appears questionable.

The fact that the negative areas increase with time in each of our experiments apparently indicates that the viscous dissipation becomes slightly less efficient in balancing the energy production as the scale of the motions increases. Any extrapolation of these results to the lower atmosphere would be highly speculative, however. In studies based upon a few temperature soundings, a ratio of 0·06 was obtained by Deardorff (1967, figure 4) for the case of cold air flowing from the eastern U.S. towards Bermuda, while a ratio of 0·4 was obtained by Lenschow & Johnson (1968, figure 8) for the diurnal heating above a Wisconsin forest. These ratios are highly uncertain because of unknown magnitudes of horizontal and vertical advection, and direct atmospheric measurements of heat flux are desirable.

If the area of negative heat flux is assumed to maintain a constant shape over short time periods as the interface rises, a simple expression relating the net cooling at the interface to its rate of rise may be obtained. In this case the mean thermal diffusion equation is

$$\frac{\partial \overline{T}}{\partial t} = -\frac{\partial}{\partial z}\left(\frac{H}{\rho c}\right) = \frac{\partial}{\partial t}\left(\frac{H}{\rho c}\right)_i \bigg/ \frac{\partial h_i}{\partial t}, \tag{6}$$

where h_i is the mean interface height. If $\partial h_i/\partial t$ is relatively much more constant than $H/\rho c$ above the interface, then the integral of (6) at any level with respect to time, from an early time until the interface reaches that level, is

$$\overline{T}_i(0) - \overline{T}_i(t) = -\left(\frac{H}{\rho c}\right)_i \bigg/ \frac{\partial h_i}{\partial t}, \tag{7}$$

where $\overline{T}_i(t)$ is the mean temperature at the interface height, and $\overline{T}_i(0)$ is the initial mean temperature at the same height. Both sides of (7) have been plotted

against t^*, and smoothed values from the right-hand side subsequently plotted in figure 10 against smoothed values from the left for the same t^*. Although qualitatively correct, expression (7), given by the solid line, underestimates the interface cooling by about 40 %. Moreover, the underestimate is made worse if account is taken of the suppression of $-(H/\rho c)_i$ caused by the 1 min time interval
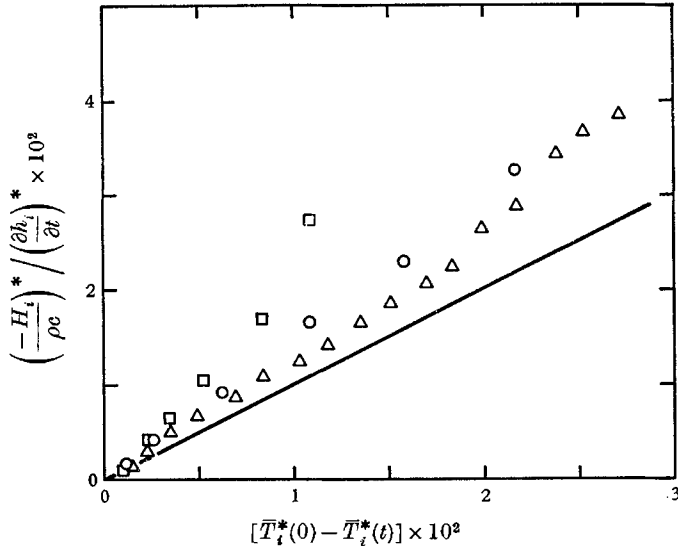

FIGURE 10. A theoretical estimate (solid line) of the total mean cooling at the level and time of mean interface passage versus the observed mean cooling (data points). $\bigcirc$, experiment A; $\square$, experiment B; $\triangle$, experiment C.

over which each heat flux curve was obtained and by time-smoothing of $\overline{T}$ profiles. From numerical tests with model profiles, we believe the suppression to be at the 50 % level for profile 3 of figure 7, but less for subsequent profiles and for experiment C. (Similarly, the ratio R was found to be underestimated, but by only 15 % and less.) The reason for the theoretical underestimate must reside in the changing shape of the negative H-region with time.

The right-hand side of (7) has been presented by Ball (1960) as an expression for the interface temperature discontinuity, rather than for the maximum mean cooling, which occurs at $z = h_i$. This interpretation will be discussed in §4.4.

4.3. *Interface height as a function of time*

The mean interface height, h_i, may be predicted as a function of time, knowing the initial lapse rate, $(\partial \overline{T}/\partial z)_0$, and the temperature difference between the heated lower boundary and its initial value, $T_{bm} - T_{b0}$. If the mixed region is approximated by a single isotherm (or adiabat), and the slight cooling above the inversion base is ignored, the rise rate is given by

$$\frac{\partial h_i}{\partial t} = \frac{\partial T_m}{\partial t} \bigg/ \left(\frac{\partial \overline{T}}{\partial z}\right)_0, \tag{8}$$

where T_m is the temperature of the mixed or turbulent region. The integral of (8) over time is

$$h_i = (T_m - T_{b0}) \bigg/ \left(\frac{\partial \overline{T}}{\partial z}\right)_0, \tag{9}$$

since $T_m = T_{b0}$ initially as a mixed layer starts to develop near the bottom.

Another relationship for h_i comes from the thermal equation, when the heat flux is assumed to decrease linearly with height from the surface to h_i:

$$\frac{\partial T_m}{\partial t} = (H/\rho c)_b / h_i, \tag{10}$$

where the small negative heat flux at $z = h_i$ has also been ignored.

If the boundary flux were constant, $\partial T_m / \partial t$ could be eliminated between (8) and (10) and the result immediately integrated to give

$$h_i = 2^{\frac{1}{2}} \left[\frac{(H/\rho c)_b}{(\partial \overline{T}/\partial z)_0}\right]^{\frac{1}{2}} t^{\frac{1}{2}}. \tag{11}$$

This $t^{\frac{1}{2}}$ dependence is the same as that found by Kato (1967) when the energy input was by a constant stress at the boundary rather than by applied heat. Kato found that

$$h_i = 1 \cdot 9 u_* \left(-\frac{g}{\rho}\frac{\partial \rho}{\partial z}\right)^{-\frac{1}{4}} (t - t_0)^{\frac{1}{2}}, \tag{12}$$

where t_0 is a small virtual displacement of the time origin. If the friction velocity, u_*, in (12) were replaced by a thermal convection velocity, w_*, given by

$$w_* = \left[g\alpha \left(\frac{\partial \overline{T}}{\partial z}\right)_0\right]^{-\frac{1}{4}} \left[g\alpha \left(\frac{H}{\rho c}\right)_b\right]^{\frac{1}{2}},$$

then (12) would be identical with (11) except for the different value of the constant of proportionality. Unfortunately there appears to be no simple means of deducing the value of the constant in (12) as there is for (11).

In our study, the lower boundary temperature was more constant than the boundary heat flux. The latter can be related to $T_{bm} - T_m$ by Townsend's (1964) dimensional argument,

$$\left(\frac{H}{\rho c}\right)_b = C \left(g\alpha \frac{\kappa^2}{\nu}\right)^{\frac{1}{3}} (T_{bm} - T_m)^{\frac{4}{3}}, \tag{13}$$

where C is a universal constant (see §4.6).

If $(H/\rho c)_b$ and h_i are eliminated between (9), (10) and (13), the resulting equation for $T_m(t)$ is

$$\frac{T_m - T_{b0}}{(T_{bm} - T_m)^{\frac{4}{3}}} \frac{\partial T_m}{\partial t} = C \left(g\alpha \frac{\kappa^2}{\nu}\right)^{\frac{1}{3}} \left(\frac{\partial \overline{T}}{\partial z}\right)_0. \tag{14}$$

Upon rearrangement, (14) may be written

$$[-(T_{bm} - T_m)^{-\frac{1}{3}} + (T_{bm} - T_{b0})(T_{bm} - T_m)^{-\frac{4}{3}}] \frac{\partial (T_{bm} - T_m)}{\partial t}$$

$$= -C \left(g\alpha \frac{\kappa^2}{\nu}\right)^{\frac{1}{3}} \left(\frac{\partial \overline{T}}{\partial z}\right)_0. \tag{15}$$

Integration of (15) then gives

$$\tfrac{1}{3}(1-T_m^*)^{\frac{2}{3}} + \tfrac{2}{3}(1-T_m^*)^{-\frac{1}{3}} = 1 + \tfrac{2}{9}Ct^*, \tag{16}$$

where T_m^* is the dimensionless temperature defined in (2) and applied to the mixed region, and t^* is the dimensionless time defined in (5). In (16) the initial condition $T_{m0} = T_{b0}$ has again been used.
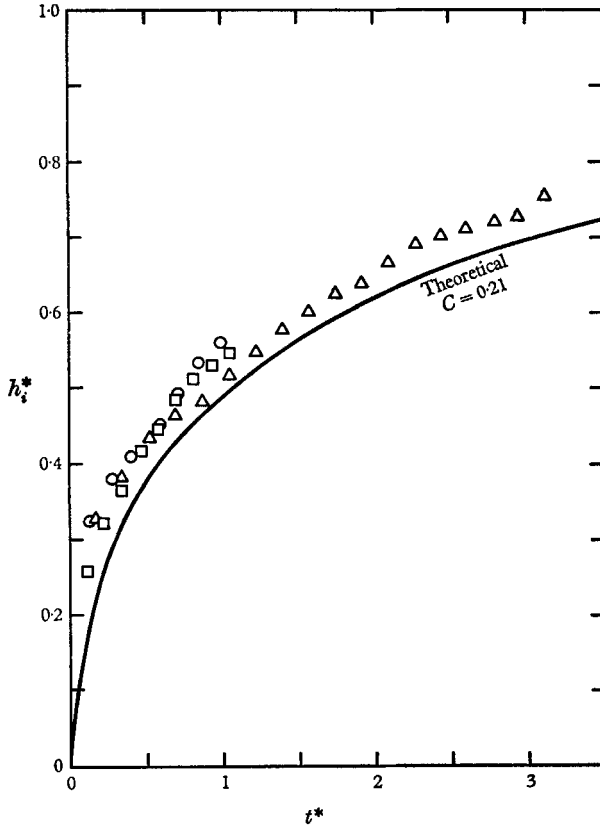

FIGURE 11. The dimensionless height of the interface, h_i^*, as function of dimensionless time, t^*. The solid theoretical curve is from equations (16) and (17). $\bigcirc$, experiment A; $\square$, experiment B; $\triangle$, experiment C.

From (2) and (9) it is also seen that

$$h_i^* = T_m^*. \tag{17}$$

Elimination of T_m^* between (16) and (17) gives h_i^* as a function of t^*, which is shown in figure 11 by the solid curve, computed for $C = 0.21$, an average value obtained for this constant. The data points give the observed interface heights, h_i^*, as a function of t^*. The theoretical underestimation of h_i^* by about 10 % is associated with its underestimation by (9), due at first to the assumption of isothermal profiles instead of the actual counter-gradient profiles, and due later also to the neglect of the interface cooling. If experimental values of T_m^* (see (17)) were plotted in figure 11, they would lie closer to the theoretical curve.

4.4. *Characteristics of the interface*

Typical photographs of the interface, obtained during an experiment when white dye (skim milk) was present in the convective region of the plexiglass tank, are shown in figures 12 and 13. This experiment corresponded roughly to run C of table 1. The portion viewed in the figures is a vertical slab about 2 cm in thickness centred near the middle of the tank. In general, the interface shape is seen to be quite complicated. At times, several or all of the following structures occur: (i) a growing dome or turret with an extremely sharp interface at its top; (ii) a flat region of rather large extent occurring after a dome or other structure has spread out or receded; (iii) a cusp-shaped region of entrainment pointing into the convective fluid; (iv) a fold on the interface which stretches out horizontally and which may leave a wisp of convective fluid within the stable layer; and (v) a breaking wave which may wrap up into a vortex. At points where the latter three structural types occur, the instantaneous interface position becomes nearly impossible to define.

Figure 12(a) (plate 1) clearly shows structures (i)–(iii) when the average interface height had reached about one-half the tank depth. Figure 12(b) (plate 1), which applies later when $h_i/h \simeq 0.8$, clearly shows an interface vortex and also an isolated convective wisp on the far left (structural types (v) and (iv)). Figure 13(a) (plate 2) is a close-up of the right-hand half of the illuminated region, and shows all structural types, except that at this time the interface domes are noticeable while flat sections are not. Figure 13(b) (plate 2), a photograph of the same area taken only a short time later, shows how the domes have flattened out, and also reveals an additional vortex at the upper left edge of the main entrainment region. From the point of view of the Helmholtz instability criterion, the appearance of breaking waves is not surprising. Neglecting the effect of viscosity, interface velocity differences of magnitude 0.5 cm sec^{-1} are sufficient to give instability to waves of length 5 cm and less.

As a result of these interesting structures the instantaneous interface in our experiments was not apparently as sharp as that reported by Rouse & Dodu (1955), who used fluids of two different densities. Even in our study, however, the interface tended to be rather well defined despite the occasional ejection of convective fluid into the base of the stable region. There are two reasons for this. First, penetration in the form of domes cannot eject convective fluid into the stable region because the restoring force of buoyancy eventually causes the fluid within the dome to recede. Yet, growing and receding domes occupy a substantial portion of the interface. Secondly, convective fluid which does get stranded by a folding of the interface can be deposited only a short distance above the interface. Before long it is entrained downwards adjacent to a dome-shaped structure, leaving only original stable fluid adjacent to the dome. The entraining fluid, of course, is not subject to a strong restoring force once it has moved into the more uniform convective region, and it is very unlikely ever to return to the stable region.

Visual observations taken when blue dye was in the stable layer generally confirmed the observations of Rouse & Dodu that entrainment occurs as wisps

streaming down from cusps adjacent to domes. The streamers typically had a maximum width of only 2 or 3 cm near the interface, tapering to a few millimetres well below the interface. Many of them descended to the bottom, moved horizontally, and then moved upwards again before disappearing from view. This complete mixing was also observed by Townsend (1964). From these observations, velocities within the convective region for run C are estimated to have been 2 cm sec^{-1} and less.

Although maximum entrainment occurred at edges of rapidly growing domes, streamers were most prevalent in the central region of the tank. This result is associated with a general circulation of rising water near the corners and walls, with sinking motion in the centre. A net circulation of this type seems to be typical of fluids heated from below and confined on the sides (Townsend 1959), and not a result of slight inequalities of surface temperature.

The local temperature structure at the interface was inferred from traces of thermocouples attached to the moving resistance-wire frame. Typical vertical traces from upward traverses of experiment A are shown in figure 3. In profile (*b*) a steep gradient at the local interface is especially evident. Sometimes no such interface was evident, from which it is surmised that the thermocouple passed through a region of entrainment. Where present, the interface discontinuity, ΔT_i, was typically of magnitude $0{\cdot}5C$. Because of the continual heating from below, ΔT_i did not increase in proportion to h_i, as would the density discontinuity in an experiment of the kind performed by Cromwell (1960) or Kato (1967).

In the penetrative convection models used by Ball (1960) and Lilly (1968), the interface irregularities were assumed to be extremely small compared with the mean interface height. The average cooling of equation (7) or figure 10, which had occurred at a given level by the time the mean interface reached that level, then would become synonomous with the temperature discontinuity across the interface, ΔT_i. Hence their models predicted that

$$\Delta T_i = -(H/\rho c)_i/(\partial h_i/\partial t) \qquad (18)$$

for the case of no subsidence and radiative or evaporative cooling.

Our measured values of ΔT_i ranged systematically from 1 to 5 times larger than the right-hand side of (18), except towards the end of experiment C, when they became smaller. Most of the theoretical underestimate can probably be attributed to the fact that the interface irregularities are not negligibly small, and that the horizontally averaged temperature profile is quite different from an individual temperature sounding. A small part of the discrepancy can be attributed to the experimental underestimate early in the experiments of $-H_i$ (discussed in §4.2).

Townsend (1964) noted that the temperature fluctuations have a maximum amplitude near the bottom of the stable region. We observe the same result in figures 14 and 15, where the root-mean-square temperature fluctuation is given as a function of time for experiments A and C, respectively. The data points were obtained as described in §3 from fixed thermocouples at two different levels, and in these two figures the overbar represents a time average. The arrows

denote our estimates of the time of passage of the mean interface level, taken here to be the time of occurrence of lowest temperature on each thermocouple trace. The maximum intensity appears to occur slightly above the interface level (before interface passage) simply because diffusive mixing, which helps smooth out the fluctuations, is present below the interface and nearly absent above. In each figure, the maximum intensity occurs at the greater height in spite of the fact that the surface heat flux is then somewhat smaller. Only in experiment A is the maximum dimensional r.m.s. fluctuation at the upper level as large as the maximum observed by Townsend (1964) upon dividing his peak-to-peak values by 6 for comparison purposes.
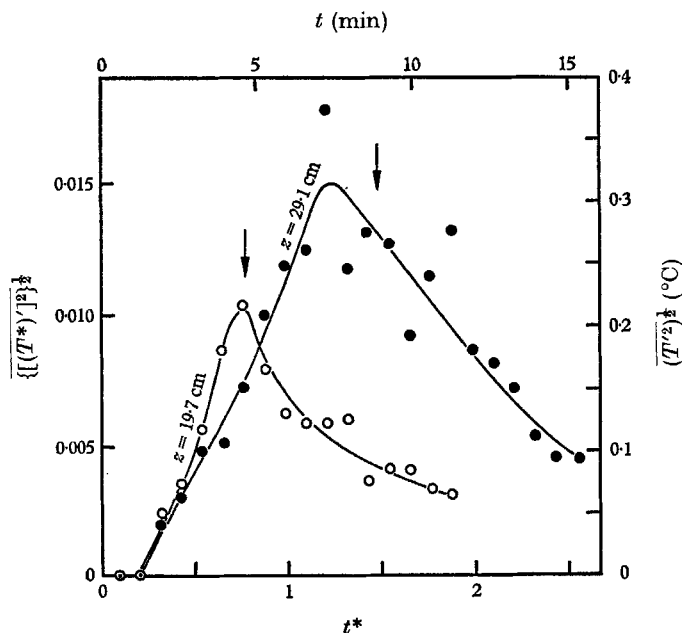

FIGURE 14. Experimental values of the standard deviation of temperature (with respect to time-averaging) as a function of time at two different locations for experiment A. Dimensionless scales are on bottom and left, dimensional scales on top and right.

From figure 14 we may obtain an estimate of the maximum vertical extent of the interface waviness or irregularity. A formula valid for internal waves is

$$\zeta = -T'/(\partial \overline{T}/\partial z), \tag{19}$$

where ζ is the vertical displacement of a particle from its initial position at rest, and T' is its associated temperature fluctuation. Applying the square of (19) to particles initially at the level of the interface when the latter has reached a height of, say, 25 cm, averaging horizontally and taking the square root, we obtain

$$(\overline{\zeta^2})^{\frac{1}{2}} = (\overline{T'^2})^{\frac{1}{2}} \bigg/ \left(\frac{\partial \overline{T}}{\partial z}\right)_0 \cong 0.7 \text{ cm}, \tag{20}$$

for experiment A. The peak displacement can be expected to have an amplitude three times this, and the maximum peak-to-trough extent is expected to be

another factor of two larger, or about 4 cm. Although this estimate incorporates several uncertainties, it agrees rather well with estimates from our visual observations. These, however, corresponded more closely to experiment *C* than to *A*. Visual estimates of the vertical extent of the interface are themselves highly uncertain because the lower interface limit estimated for regions of entrainment is an arbitrary matter. If the value of 4 cm is centred at the interface level of curve 5 in figure 7, most of the region of negative heat flux falls within this interval. The inference to be drawn is that the entrainment process, which requires a contorted interface for its existence, can probably explain all but a small 'tail' (at higher levels) of the negative heat flux observed.
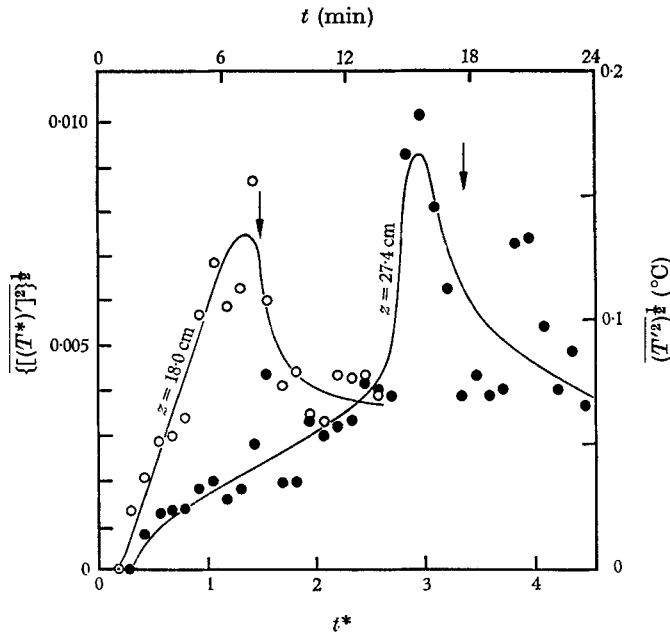

FIGURE 15. Same as figure 14, but for experiment *C*.

4.5. *The stable region*

Temperature measurements from fixed thermocouples well within the stable region showed rather regular oscillations having the appearance of internal gravity waves. A typical record at height 29·1 cm for experiment *A* is shown in figure 16. As noticed by Townsend (1964) the wave-induced fluctuations well above the interface are not skewed or asymmetric as they are in much of the convective region. However, at times 7·7, 8·2 and 8·9 min asymmetric cold peaks occur. These must have been associated with the close approach from below of relatively cold interface domes which subsequently receded. At 8·9 min an interface dome appears to have moved slightly above the thermocouple for a few seconds. (Presence of the convective region is inferred from relatively high frequency fluctuations indicative of small-scale motions and significant molecular smoothing.) After about 9·2 min the interface appears to have passed and to have

remained above the thermocouple except perhaps for brief retrogressions centred at 10·0 and 10·6 min. Between 11 and 12 min, some reverse asymmetry is present, and is probably associated with narrow streamers of warm fluid entraining downwards. A net cooling at the thermocouple preceding the interface passage is evident between about 6·7 and 9·2 min.
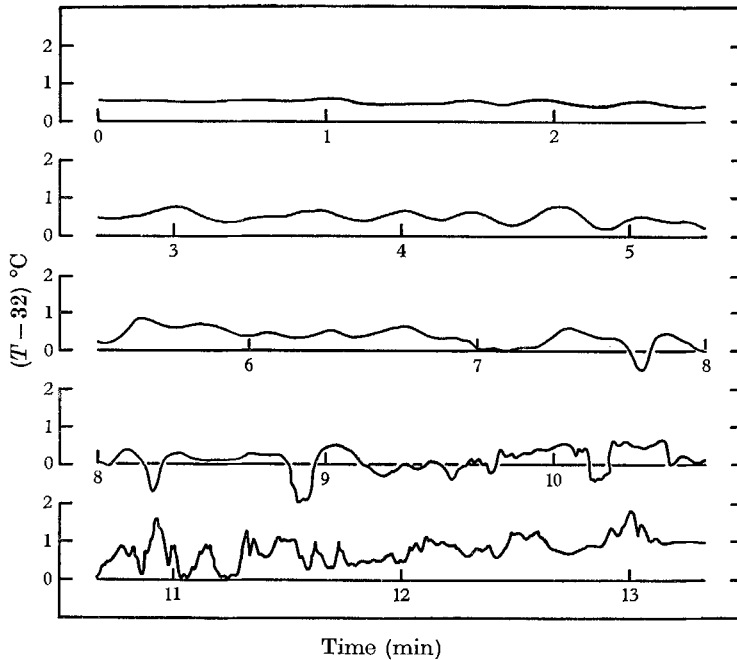

FIGURE 16. A record of thermocouple temperature versus time at a height of 29 cm (experiment *A*).

The initial period of the internal waves is seen to be about 25 sec in figure 16. This period is considerably longer than the Brunt–Väisälä period of 17·4 sec, listed in table 1. Longer periods are theoretically expected to be associated with waves whose vertical structure is sinusoidal in character, with a nodal plane at the upper boundary (Phillips 1966, p. 164). Shorter periods are associated with waves which decay with height nearly exponentially at a rate proportional to the difference between the Brunt–Väisälä period and the actual enforced period. Hence, the convectively forced waves of short period cannot become evident until the interface is relatively close to the thermocouple. This qualitative behaviour is apparent in figure 16, although a rigorous analysis of the internal wave motion should allow for the fact that the coefficient of thermal expansion of water varies considerably with temperature, even at temperatures well above 4 °C.

The intensity of the temperature fluctuations induced by internal waves shows an interesting difference in figures 14 and 15. In the former case (experiment *A*), in which the interface rose quite rapidly, significant fluctuations first occurred at about the same time at both heights of measurement, and increased initially at about the same rate. In figure 15 (experiment *C*), associated with a

more slowly rising interface, the fluctuations occurred earlier at the lower level and increased much more rapidly there, until interface passage, than at the higher level. This latter behaviour means that $\overline{T'^2}$ decreased rapidly with height well above the interface level, in agreement with Townsend's (1964) steady-state data. On the other hand, the more uniform vertical distribution of $\overline{T'^2}$ of our experiment A, well above the interface, implies a greater relative amplitude of internal waves with sinusoidal-type vertical dependence in this case. This in turn implies a frequency spectrum of vertical velocities in the convective region having greater intensity at lower frequencies than in experiment C. This conclusion is plausible in view of the greater heat flux in experiment A than in C.

The net cooling at a point above the interface in figure 16, and the small tails to the negative heat flux curves of figures 7–9, which apparently extend above the highest level reached by any portion of the local interface, require some discussion. (The tails probably were suppressed late in each experiment by our assumption of constant mean temperature at $z = 32 \cdot 4$ cm.) In the absence of any evident small-scale mixing or wave-breaking this far above the interface, it might be thought that internal gravity waves should not have been responsible. However, inspection of the thermal-variance equation

$$\frac{\partial}{\partial t}\left(\frac{\overline{T'^2}}{2}\right) + \overline{w'T'}\frac{\partial \overline{T}}{\partial z} + \frac{\partial}{\partial z}\left(\frac{\overline{wT'^2}}{2}\right) = 0 \tag{21}$$

as applied to the horizontally homogeneous case with negligible thermal diffusion indicates that a heat transport by (finite-amplitude) internal waves could be supported by non-steady conditions and/or by vertical divergence of $\frac{1}{2}\overline{wT'^2}$. The non-steady term in (21) is of the proper sign to support a negative heat flux above the interface where $\overline{T'^2}$ increases with time. Since the rate of increase is largest close to the interface, the vertical divergence of the associated flux would furthermore produce a cooling as observed. However, the magnitude of $(\partial/\partial t)(\overline{T'^2}/2)$, which can be obtained from figure 14, was found to be nearly an order of magnitude too small to produce the magnitude of negative flux observed in the tails. Hence the triple-correlation term, $(\partial/\partial z)(\frac{1}{2}\overline{wT'^2})$, is probably responsible, but no convincing explanation for its sign or magnitude is available. The quantity $\overline{wT'^2}$ evidently is negative near the interface and approaches zero with increasing height.

Two other possible explanations for the cooling and small negative heat flux in this region were considered but rejected from order-of-magnitude arguments. First, descending motion adjacent to the imperfectly insulated walls may have resulted in a slight upward transport within the main body of fluid covered by the resistance wire. Secondly, a bulk rising motion of the slowly warming and expanding water in the convective region may have caused the water above to lift slightly with respect to a reference height of the resistance wire, and thus advected cooler water upwards. Both effects, though undoubtedly present, seem to have been entirely insignificant.

4.6. Boundary heat flux

It is of interest to compare Townsend's value of C in (13), obtained for statistically steady thermal convection of air in an open box, with the values from our non-steady experiment using water in an enclosed tank. The temperature of the mixed region, T_m in (13), was taken to be the lowest existing mean temperature. Actual values of T_b were used, rather than values of T_{bm}. The quantities κ, ν and α were evaluated at a temperature midway between that of the lower boundary and that of the mixed region, and $(H/\rho c)$ was taken from figures 7–9. Resulting values of C are shown in table 2. There is a definite trend toward lower values with increasing time, even if the first three values in each experiment are rejected on the grounds of too much time-smoothing of $\bar{T}$ profiles. We have no explanation for this trend, but note that values near the ends of the experiments, when conditions were most steady, lie between 0·18 and 0·21. The average of these agrees well with the value 0·193 found by Townsend, but perhaps only coincidentally. If we had evaluated ν and α at the boundary temperature, our C values would be about 7 % smaller.

It might be noted that (13) may not hold well for Prandtl numbers differing strongly from unity. The $\frac{1}{3}$-dependence of κ^2/ν stems from the observation that the Nusselt number in parallel-plate convection is dependent upon the $\frac{1}{3}$-power of the Rayleigh number and the assumption that it is independent of Prandtl number. This assumption is not quite correct according to the weak effect of Prandtl number which has been measured by Globe & Dropkin (1958). The Prandtl number in the present experiments ranged from about 7 at cooler temperatures to about 4 at the highest temperature; in Townsend's open-box experiment it was 0·7.

5. Summary and conclusions

Laboratory experiments of non-steady penetrative convection in water were performed which closely simulate, except for scale, the lifting of an atmospheric inversion above heated ground. The horizontally averaged temperature was found to vary smoothly with height and to undergo a slight cooling just above the inversion base. The maximum cooling was related to the downward heat transport at the inversion base and to the rise rate of the latter. The vertically integrated negative heat flux near the inversion base was only about 1·5 % of the vertically integrated upward flux below.

The local interface between the stable region and the convective region stayed rather well defined throughout the experiments. The interface shape is a combination of forms: domes with adjacent cusps through which downward entrainment occurs, flat sections, folded structures and breaking waves. The height of the mean level of the interface was quantitatively related to the boundary heat flux, the lapse rate in the stable region, and the elapsed time.

Values of the universal constant which relates the boundary heat flux to the temperature difference between the boundary and the well-mixed region support the value found earlier by Townsend.

REFERENCES

BALL, F. K. 1960 Control of inversion height by surface heating. *Quart. J. Roy. Meteor. Soc.* **86**, 483–94.

CROMWELL, T. 1960 Pycnoclines created by mixing in an aquarium tank. *J. Mar. Res.* **18**, 73–82.

DEARDORFF, J. W. 1967 Empirical dependence of the eddy coefficient for heat upon stability above the lowest 50 m. *J. Appl. Meteor.* **6**, 631–43.

GLOBE, S. & DROPKIN, D. 1958 Natural convection heat transfer in liquids confined by two horizontal plates and heated from below. *1958 Heat Transfer and Fluid Mechanics. Inst. Berkeley: Univ. of Calif.* pp. 156–65.

IZUMI, T. 1964 Evolution of temperature and velocity profiles during breakdowns of a nocturnal inversion and a low level jet. *J. Appl. Meteor.* **3**, 70–82.

KATO, H. 1967 On the penetration of a turbulent layer into stratified fluid. *The Johns Hopkins Gravitohydrodynamics Laboratory* Rep. no. 2, October 1967. Baltimore, Maryland.

KRAUS, E. B. & TURNER, J. S. 1967 A one-dimensional model of the seasonal thermocline. Part II. The general theory and its consequences. *Tellus*, **19**, 98–106.

LENSCHOW, D. H. & JOHNSON, W. B. 1968 Concurrent airplane and balloon measurements of atmospheric boundary-layer structure over a forest. *J. Appl. Meteor.* **7**, 79–89.

LETTAU, H. H. & DAVIDSON, B. 1957 *Exploring the Atmosphere's First Mile.* Vols. 1 and 2. New York: Pergamon.

LILLY, D. K. 1968 Models of cloud-topped mixed layers under a strong inversion. *Quart. J. Roy. Meteor. Soc.* **94**, 292–309.

PHILLIPS, O. M. 1966 *The Dynamics of the Upper Ocean.* Cambridge University Press.

PRIESTLEY, C. H. B. 1959 *Turbulent Transfer in the Lower Atmosphere.* University of Chicago Press.

ROUSE, H. & DODU, J. 1955 Turbulent diffusion across a density discontinuity. *La Houille Blanche*, **10**, 522–32.

TELFORD, J. W. 1967 The convective mechanism in clear air. *J. Atmos. Sci.* **23**, 652–66.

TOWNSEND, A. A. 1959 Temperature fluctuations over a heated horizontal surface. *J. Fluid Mech.* **5**, 209–41.

TOWNSEND, A. A. 1964 Natural convection in water over an ice surface. *Quart. J. Roy. Meteor. Soc.* **90**, 248–59.

TURNER, J. S. & KRAUS, E. B. 1967 A one-dimensional model of the seasonal thermocline. Part I. A laboratory experiment and its interpretation. *Tellus*, **19**, 88–97.

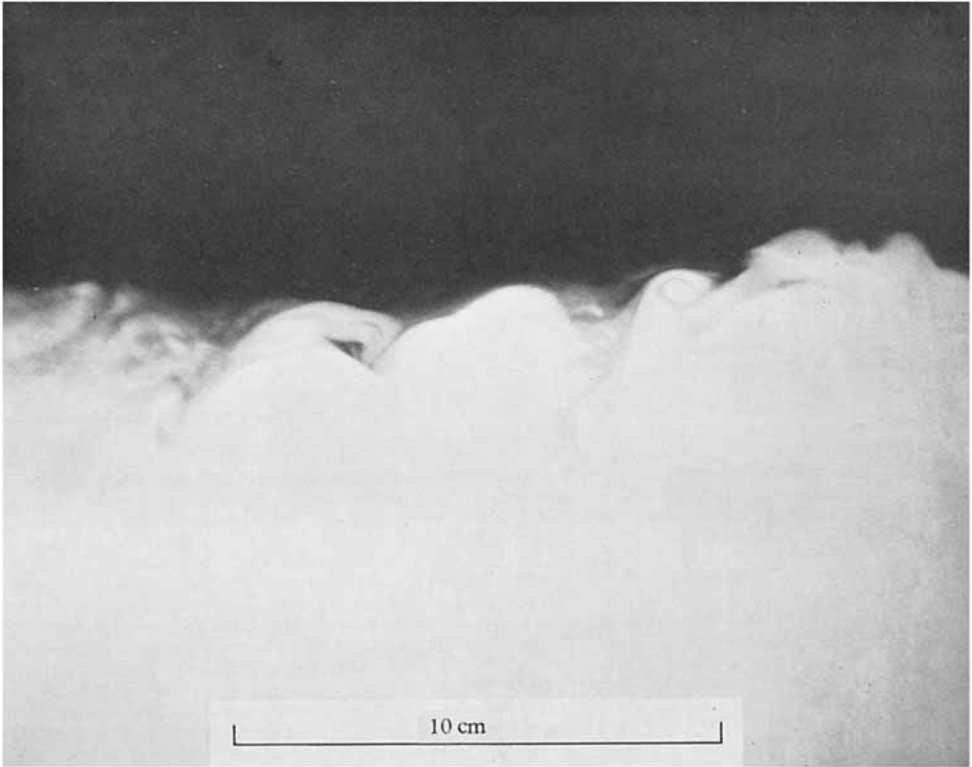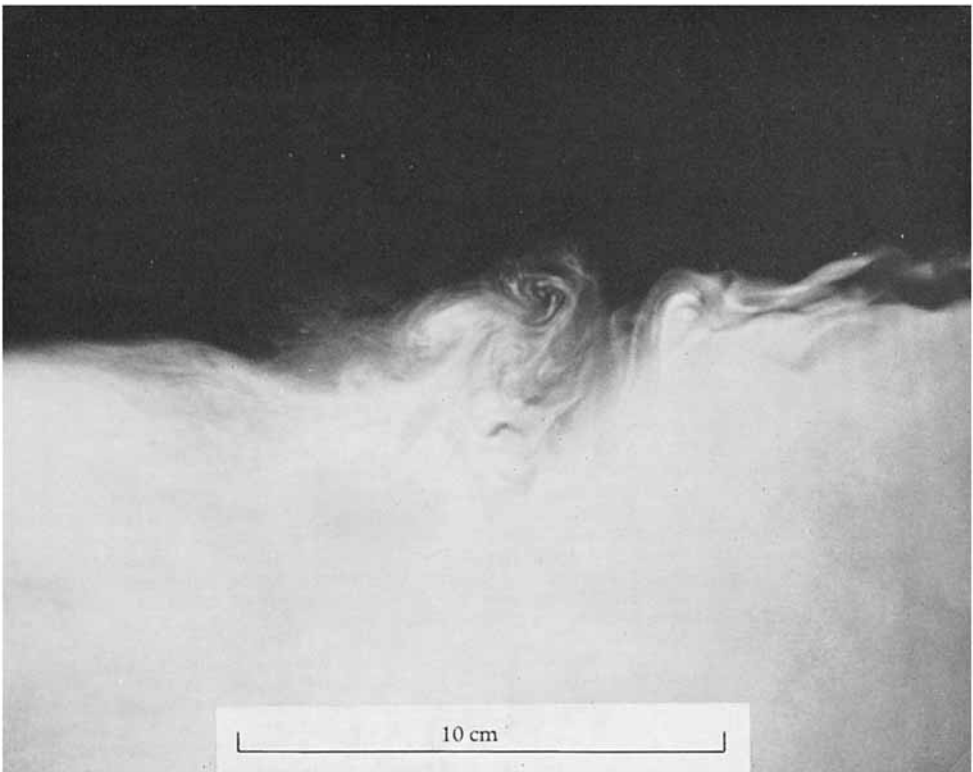VERONIS, G. 1963 Penetrative convection. *Astrophys. J.* **137**, 641–63.
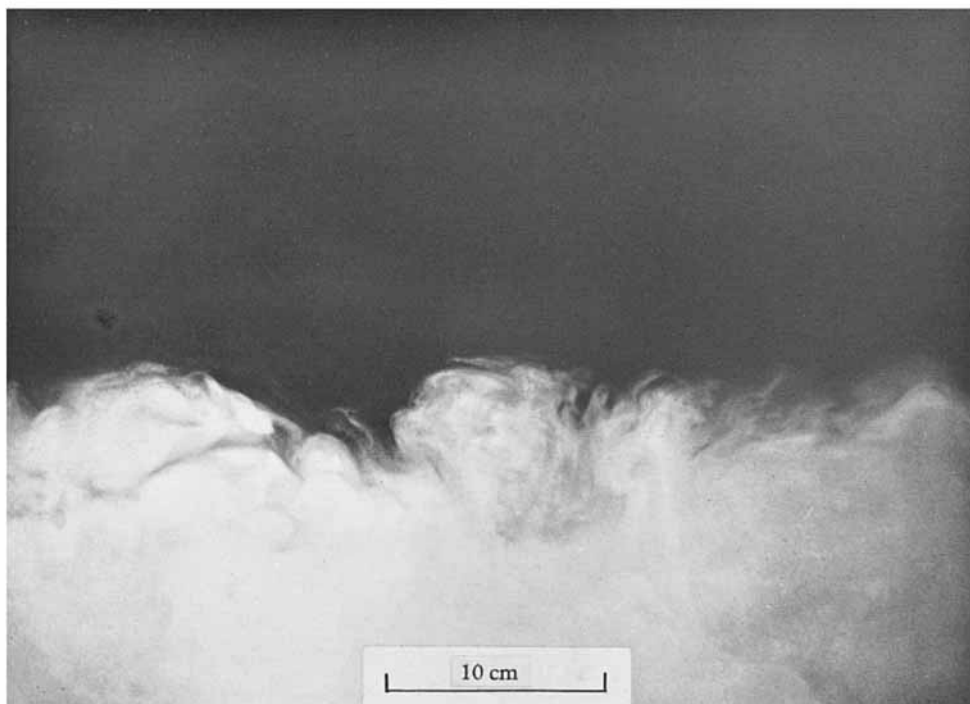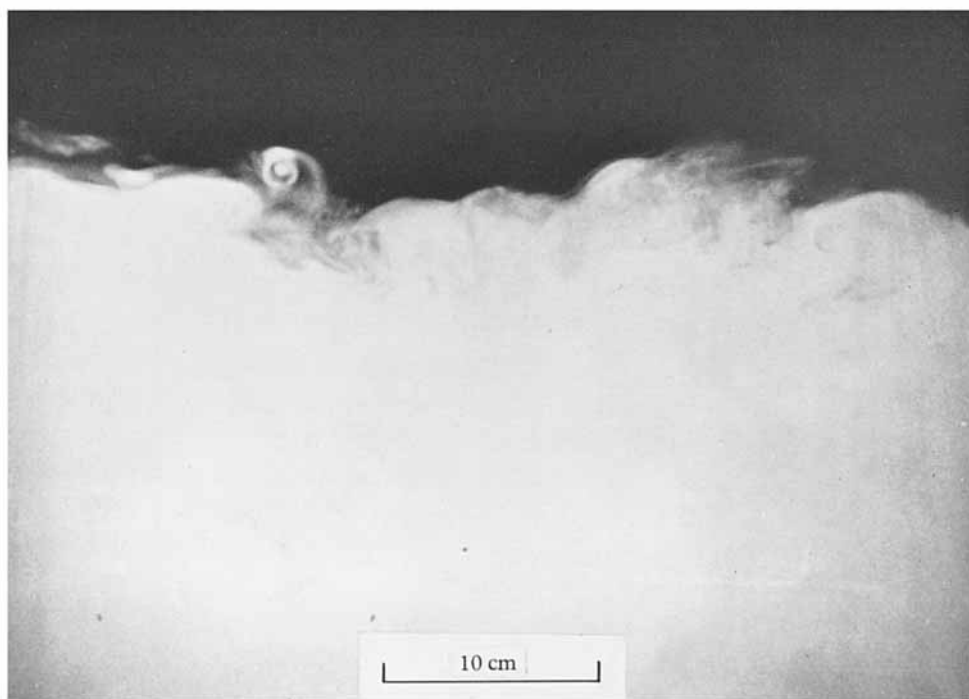
FIGURE 12. Photographs of the convective region and interface within the tank of width 50 cm and height 35 cm, with conditions similar to those of experiment C. (a) Mean interface height about 17 cm. (b) Mean interface height about 28 cm.

(a)

(b)

FIGURE 13. Close-up photographs of the convective region and interface during the same experiment as in figure 12. (a) Interface domes sharply outlined. (b) Interface more diffuse.

DEARDORFF, WILLIS AND LILLY